Contents lists available at ScienceDirect

Fuel

journal homepage: http://ees.elsevier.com

NO_x emission and thermal performances studies on premixed ammonia-oxygen combustion in a CO_2-free micro-planar combustor

Tao Cai [a], Dan Zhao [a,*], Bing Wang [b], Junwei Li [c], Yiheng Guan [d]

[a] Department of Mechanical Engineering, University of Canterbury, Christchurch 8140, New Zealand
[b] School of Aerospace Engineering, Tsinghua University, Beijing, China
[c] School of Aerospace Engineering, Beijing Institute of Technology, Beijing, China
[d] School of Energy and Power Engineering, Jiangsu University of Science and Technology, Mengxi Rd 2, 212003 Zhenjiang City, Jiangsu Province, China

ARTICLE INFO

Keywords
Carbon-free fuel
NO_x emission
Ammonia
Thermodynamics
Heat transfer

ABSTRACT

Unlike hydrocarbon fuel, ammonia is a carbon-free and renewable energy source. It is also regarded as one of the potential energy carriers. However, ammonia combustion for power generation is not well studied under micro-scale conditions, especially concerning nitrogen oxides (NO_x) emission. For this, thermal performances and NO emission characteristics of premixed ammonia/oxygen combustion are numerically investigated on a micro-planar combustor. The effects of 1) the equivalence ratio ϕ, 2) inlet temperature T_{in} and 3) inlet pressure P_{in} are examined. The outer wall mean temperature (OWMT) is found to vary non-monotonically as the mixture varies from lean to rich conditions, with the peak occurring at $\phi = 0.9$ mainly due to the optimal heat transfer performance. However, a low ϕ could lead to the high nitric oxides (NO) concentrations because of the high flame temperature as well as O atom concentrations. Up to 75.5% of NO reduction could be achieved, as ϕ is optimized. Furthermore, increasing T_{in} is shown to be associated with a low OWMT and NO concentration. In addition, varying P_{in} is shown to lead to not only OWMT being changed but also NO formation being mitigated. The decrease in NO concentration for high P_{in} is mostly attributable to the short residence time of high flame temperature in the channel and low OH concentrations. This work reveals that optimizing the operating thermodynamic parameters is an effective means to reduce NO emissions and improve thermal performances.

1. Introduction

Due to the stringent emission regulation and the demand for reducing independence on fossil fuel, there is of great interest in searching for an alternative fuel. Some potential candidates are being proposed and tested, such as biogas, hydrogen and ammonia [1–3]. Among these, hydrogen is highly recommended since there is no formation of greenhouse gases such as carbon dioxide (CO_2). The product from hydrogen combustion is water only. Unfortunately, there are several technical challenges in using H_2 as a fuel in terms of storage and transport. H_2 is highly volatile with a low flash point and high laminar burning velocity [4], resulting in the fact that it is difficult to be stored and transported. These could render the wide usage of H_2 in practice. In contrast, NH_3, another promising energy carrier with carbon-free characteristics [5–7], can be easily stored in the liquid state at 293 K and 8.0 atm. Furthermore, the transport infrastructure for NH_3 in some countries is well built. Apart from these merits, the production process of NH_3 is quite mature with the most widely used one being the Haber-Bosch process. Meanwhile, some eco-friendly and feasible approaches to produce ammonia have been proposed and demonstrated by using solar energy, wind energy and etc. [2,8,9]. These features make it more attractive in using ammonia for energy-conversion systems in comparison with H_2.

The idea of using ammonia as a fuel for internal combustion engines was first proposed in 1905. Inspired by this, the first application powered by ammonia was produced in Belgium in 1942 [10]. Later extensive research has been conducted on the internal combustion engines fueled with ammonia [11–16]. Duynslaegher et al. [14] numerically explored the effect of pressure and temperature on the emission performance of ammonia premixed combustion. It was confirmed that the equivalence ratio played a significant role in nitrogen monoxide generation, while the compression ratio and temperature had less effects on the formation of NO as the equivalence ratio was beyond unity. Westlye et al. [16] experimentally demonstrated that the nitric oxide emissions from combustion of ammonia in a spark ignition engine will be lower than from hydrocarbon combustion near stoichiometric condi-

* Corresponding author.
E-mail address: dan.zhao@canterbury.ac.nz (D. Zhao)

https://doi.org/10.1016/j.fuel.2020.118554
Received 14 January 2020; Received in revised form 25 May 2020; Accepted 26 June 2020
Available online xxx
0016-2361/

tions. Meanwhile, a number of studies involved with co-combustion such as ammonia-hydrogen/gasoline/diesel have also been implemented for heavy duty engines [16–22]. Mørch et al. [19] conducted a series of experiment to assess the influence of blending various ammonia to hydrogen ratios. Result showed that mixture with 10% hydrogen on a molar basis owned the best performance in terms of efficiency and power. Ryu et al. [21] experimentally examined the effect of ammonia addition on the combustion performance in a spark-ignition engine. It was found that adding ammonia can result in not only the reduction in CO emissions, but also the increase in NO_x and HC formation. In addition, the working performance of using ammonia in a compression-ignition engine was assessed by Reiter and Kong [22]. It was demonstrated that the addition of ammonia had the potential to improve the power output without increased NO_x emissions, as the energy substitution was under a reasonable range.

Furthermore, there are increasing interest in applying ammonia for gas turbine engines in recent years [23–29]. For the first time, Kurata et al. [24] experimentally demonstrated the successful implementation of the ammonia-air power generation using a 50 kW class gas turbine system. Somarathne et al. [27] explored the emission characteristics of ammonia/air turbulent flames in a swirl combustor under high pressure conditions. Results indicated that the local NO concentration strongly depended on the local OH concentration. It was also found that NO_2 and N_2O generally followed the NO emission characteristics with respect to $\phi_{\text{global/pri}}$. At $\phi = 1.1$, the minimal NO, NO_2 and N_2O emissions can be observed, and there were little NH_3 emissions at the combustor outlet. In addition, a series of approaches to enhance ammonia combustion have been put forward and tested such as blending fuels with a high laminar burning velocity [24,30–34] as well as elevated temperature and pressure. Valera-Medina et al. [32] carried out a preliminary investigation on the ammonia-hydrogen combustion in swirling gas turbine combustors. The operability range of pure ammonia was found to be narrower compared with those of blended fuels due to the high diffusivity of hydrogen, and the excess production of OH and O was responsible for the high NO_x emissions.

Apart from these applications discussed above, attempts to adopt ammonia as a fuel for micro-power systems have been made [35–39]. The flow field, flame structure as well as emission performances of CH_4-NH_3-air combustion in micro gas-turbine combustors were examined by Okafor et al. [36] experimentally and numerically. The optimum equivalence ratio for reducing NO_x was found to vary from 1.30 to 1.35 depending on the ammonia fraction. Nakamura et al. [38] investigated the combustion and ignition characteristics of ammonia/air in a temperature-controlled micro-combustor. They proved the capability of applying ammonia for micro-power systems. Furthermore, Okafor et al. [39] demonstrated that there was a possibility of stable power generation in an ammonia-fueled micro gas turbine with a high combustion efficiency. Forgoing studies reveal that ammonia has a great potential to be used as a renewable and alternative fuel in the many practical fields in the future. Unlike conventional industry-scale gas turbine combustion, combustion occurring under micro-scale conditions is associated with two major challenges [40]. First, the flame is involved with a large heat loss as a result of the large surface-to-volume ratio. This could result in the flame thermal/radical quenching easily. Second, incomplete combustion may occur, because of the reduced residence time resulting from the micro-scale dimension of the combustor. Therefore, some interesting characteristics of ammonia combustion in a micro-combustor are believed to take place. This partially motivated the present work. The insights on the fundamental NH_3-fueled micro-combustion characteristics is meaningful and rewarding, which can be used to guide the experimental studies. However, to the best of the present authors' knowledge, there are little literature review discussing the ammonia flame in a micro-planar combustor. This also partially motivated the present work.

In this work, three-dimensional numerical simulations are performed to shed light on the fundamental thermal and emission characteristics of ammonia-fuelled micro-combustion with varying thermodynamic properties. Given the low laminar burning velocity, it is difficult to ignite ammonia/air. As a result, the oxygen is chosen as the oxidizer. The numerical model is described in Section 2. The simplified geometric model is illustrated. Governing equations involving the combustion-flow-heat transfer-mas transfer process are described. Comparison of grid independence and mechanism are implemented. The effects of the equivalence ratio ϕ, inlet temperature T_{in} as well as inlet pressure P_{in} on the fundamental combustion and emission characteristics are discussed in Section3. Key findings are summarized in Section 4.

2. Numerical approach

2.1. Geometric model

The geometry of the micro-planar combustor with a cross-section of a rectangular-shaped is schematically illustrated in Fig. 1. The overall geometry of the combustor in the x, y, z directions are 20 mm, 11 mm and 3 mm. Since the wall thickness is 0.5 mm, the channel length, width and height are 20 mm, 10 mm and 2 mm respectively. According to the previous study [38], the quenching diameter of ammonia/air combustion is large than 2 mm. Therefore, it is reasonable to define the term of "micro-scale combustion" for combustion used in the present

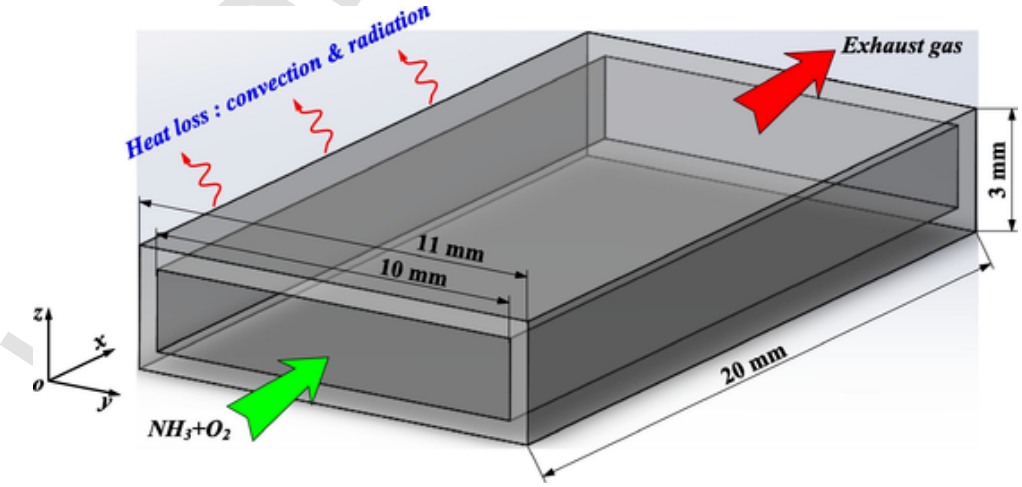

Fig. 1. Schematic of the simplified micro-planar combustor.

work. This is because the characteristic length scale is closely related to "flame quenching diameter". The combustor is assumed to be made of Steel. Such material is proven capable of withstanding a high temperature.

2.2. Governing and species conservation equations

In this work, ANSYS (Fluent 18.1) is adopted to systematically solve all the governing equations. The detailed chemistry mechanism for ammonia/oxygen combustion involves 22 elementary species and 67 reversible reactions [41]. The pressure-velocity coupling is solved using SIMPLE algorithm, whilst the governing equations and species are discretized by the second-order upwind scheme. The convergence criterions for all residuals are set less than 10^{-6}. The steady-state mass conservation, momentum conservation, energy balance, and species equations in the gas phase as well as conjugated heat conduction within the solid walls are as follows:

Continuity:

$$\frac{\partial}{\partial x_i}\left(\rho u_i\right) = 0 \tag{1}$$

Momentum:

$$\frac{\partial}{\partial x_j}\left(\rho u_i u_j - \tau_{ij}\right) = -\frac{\partial p}{\partial x_i} \tag{2}$$

Energy:

$$\frac{\partial}{\partial x_j}\left(\rho u_i h + F_{h,j}\right) = u_j \frac{\partial p}{\partial x_j} + \tau_{ij}\frac{\partial u_i}{\partial x_j} \tag{3}$$

Species:

$$\frac{\partial}{\partial x_j}\left(\rho u_j m_l + J_{l,j}\right) = R_l \tag{4}$$

Conjugated heat conduction:

$$\frac{\partial(k\partial T_w)}{\partial x^2} + \frac{\partial(k\partial T_w)}{\partial y^2} + \frac{\partial(k\partial T_w)}{\partial z^2} = \frac{\partial(\rho_w c_w T_w)}{\partial x^2} \tag{5}$$

where ρ is the density, u_i is the velocity components of i direction (i = 1, 2, 3), p denotes the pressure, τ_{ij} denotes the stress tensor, h represents the total enthalpy, $F_{h,j}$ represents the energy flux of the x_j direction, m_l stands for the mass fraction of species$l$, $J_{l,j}$ stands for the diffusion flux of species$l$ in the direction, R_l is the production rate of species$l$ by chemical reaction, k, ρ_w and c_w are the thermal conductivity, density and specific heat capacity of the solid material, respectively, T_w denotes the temperature of the outer wall.

Considering the fact that the maximum Reynolds number based on the non-reacting flow field is 306, a laminar model is chosen to simulate the flow of the mixture in the combustor, and a finite-rate model is adopted for chemical reaction. When calculating the properties for the fuel-oxy mixture, the specific heat is solved based on the mixing-law whilst the ideal-gas-mixing law is used for both the thermal conductivity and viscosity [42]. Regarding the individual species, the specific heat is calculated according to piecewise-polynomial in terms of temperature, while the thermal conductivity and viscosity are computed by kinetic-theory [42]. For mass and energy diffusion, the Soret effect plays an important role in affecting the flame speed, while the Dufour effect is normally negligible [43]. Therefore, the Soret effect is modeled only to save the computational time. The NO_x model is not compatible with premixed combustion and thus is not considered in the processes of numerical simulations. Furthermore, the pressure diffusion is also neglected due to their small magnitude. The radiation between the inner surface and mixture is calculated by using the discrete ordinate model [44].

The boundary conditions are specified as follows. A uniform velocity profile with an initial temperate of 300 K is assumed at the inlet of the micro-combustor, and the operating pressure is 101, 325 Pa unless otherwise stated. Note that the inlet temperature and operating pressure are varied for the purpose of comparison in this work. Pressure-outlet boundary condition is considered at the combustor outlet. With regards to the interior surfaces between the gas and the combustor walls, zero diffusive flux species and no slip boundary condition are considered [45]. The heat loss rate associated with radiation and convection heat transfer from the external walls is calculated by the Eq. (6):

$$q = h\left(T_W - T_\infty\right) + \varepsilon\sigma_b\left(T_W^4 - T_\infty^4\right) \tag{6}$$

where h represents the natural convection heat transfer coefficient (20 $W/m^2 \cdot K$ [46,47]); T_W is the outer-wall temperature; T_∞ is the ambient temperature (300 K); ε denotes the emissivity of the solid surface (0.85); σ_b denotes the Stephan-Boltzmann constant ($5.67 \times 10^{-8} W/m^2 \cdot K^4$).

2.3. Grid independence and mechanism comparison

To ensure the accuracy of calculated results and limit the computational costs, the mesh independence study is performed. Three types of meshes are generated using the Gambit 2.4.6, corresponding to the coarse (cells: 89,000), medium (cells: 168,000) and fine meshes (cells: 352,000). Fig. 2 presents the centerline temperature profiles on the cross section of the combustor along the axial direction using three different number of grid cells, when the NH_3 volume flow rate is 400 mL/min and ϕ = 1.0. It can be seen from the figure that the centerline temperatures show the same trend, no matter what type of mesh is applied. It is, however, worthwhile noting that there are significant differences in the peak centerline temperatures and its locations for the coarse and medium mesh. By contrast, these deviation are negligible when it comes to the medium and fine mesh. This indicates that the medium mesh can satisfy the computational requirement and is therefore selected for the following numerical simulations.

Currently, the device to diagnose the ammonia combustion that occurs under micro-scale conditions is not available, and thus it is not possible to validate the accuracy of computational model. This is why the computational results predicted by the present reduced chemical mechanism are compared to those obtained from a much detailed one developed by Nakamura et al. [37]. They demonstrated the applicability of ammonia combustion in a micro flow reactor using the detailed

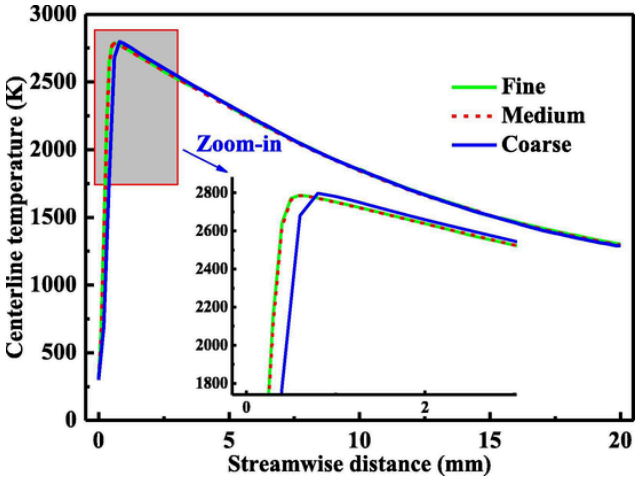

Fig. 2. Comparison of centerline temperature profiles on the cross section of the combustor in the axial direction, as the mesh number is set to 3 different values.

mechanism. In general, a detailed reaction mechanism is more effective in capturing the combustion characteristics than a reduced one. Unfortunately, this requires a great amount of computational time and cost. Therefore, adopting a reduced chemical reaction mechanism capable of reflecting the combustion phenomena similar to those with a detailed one is more suitable. From the computations the concentrations of nitrogen dioxide (NO_2) and nitrous oxide (N_2O) in the flame are found to be negligible compared to NO. Similar results were also confirmed numerically and experimentally in previous works [48,49]. Consequently, more attentions are paid on NO production and it is thus regarded as an indicator for NO_x emissions.

Fig. 3 shows the computed results using the two chemical reaction mechanisms from Drake and Blint [41] and Nakamura et al. [37] in terms of outer wall mean temperature (OWMT) and NO mole fraction at the combustor outlet, as the equivalence ratio ϕ is 1.0 and NH_3 volumetric flow rate is set to 4 different values. It can be seen from the figure that there is an excellent agreement in OWMT, and the maximum relative error is only 1.3%, as the ammonia volumetric flow rate is 400 mL/min. However, there are some differences in NO concentrations. The relative large deviation in the NO mole fraction calculated from the Nakamura's and Drake's mechanisms may be mainly due to the fact that the former one underestimates the NO formation. Despite the relative error in predicting the NO formation, the results calculated by using the two reaction mechanisms generally show the similar tendency as a function of the fuel flow rate, thus indicating that the reduced reaction mechanism used in the present work is sufficiently accurate to capture the basic combustion characteristics of ammonia micro-flame.

3. Results and discussion

3.1. Effect of the equivalence ratio ϕ

Thermal performances of a micro-planar combustor play a critical role in determining the power output of a micro-power generation system. Thus the effect of varying the equivalence ratio ϕ on the outer-wall mean temperature (OWMT) is investigated, as shown in Fig. 4. It can be seen from this figure that OWMT varies monotonically with varied the fuel flow rate. Increasing the fuel flow rate leads to the OWMT being increased, irrespective of ϕ. This is particularly reasonable because of the large heat release rate when the complete combustion occurs. Another feature shown in Fig. 4 is that for a specified fuel flow rate, OWMT is increased first and then decreased with elevated ϕ. For example, there is considerable increase of OWMT when increasing ϕ from 0.8 to 0.9; further increasing ϕ results in a drop of OWMT. The reasonable explanation for the phenomenon is that for a specified fuel flow rate, decreasing the fuel/oxidizer ratio results in the mixture inlet velocity being increased. The increased inlet velocity affects the combustion process in two aspects. One is associated with the reduced residence time which has a negative impact on the chemical reactions. Another one is the enhanced heat transfer between the inner gases and walls. The combined effects determine the heat transfer characteristics inside the micro-combustor. The value of ϕ with the highest OWMT is 0.9, implying that under which condition the residence time for heat transfer is optimal.

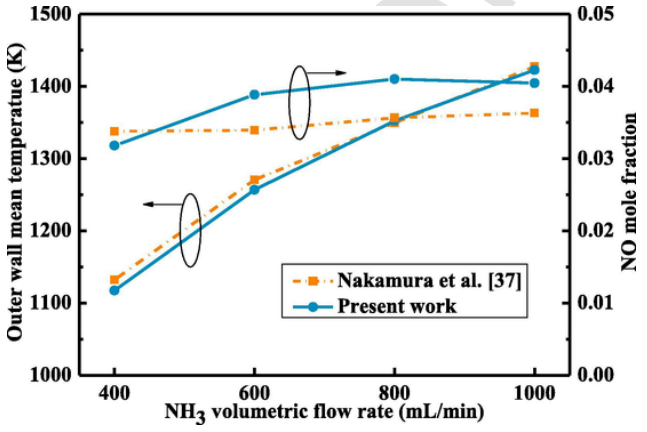

Fig. 3. Comparison of computed mean temperature of outer wall and NO mole fraction at the combustor outlet varied with NH_3 volumetric flow rate using two different kinetic mechanisms. One is from Ref. [37], and the other mechanism is discussed by Drake and Blint [41].

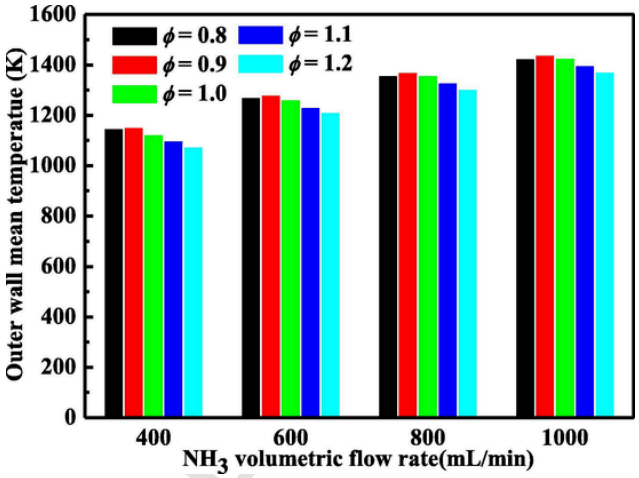

Fig. 4. Comparison of OWMT as a function of the NH_3 volumetric flow rates at various ϕ.

Fig. 5 illustrates the mole fraction of NO at the combustor outlet, as ϕ is set to 5 different values ranging from 0.8 to 1.2. It can be seen that the NO formation strongly depends on the equivalence ratio ϕ. The NO concentration is decreased dramatically as ϕ is increased, irrespective of the NH_3 volumetric flow rate. The predicted NO concentration with ϕ = 1.2 is only 24.5% of those for ϕ = 0.8, when the NH_3 volumetric flow rate is 400 mL/min. Furthermore, it is worth noting that for a fixed value of ϕ, there is a moderate increase in the NO mole fraction, as the NH_3 volumetric flow rate is increased from 400 mL/min to 600 mL/min. These variations, however, are relatively smaller, as the fuel flow rate is further elevated, implying that the NO production rate is less sensitive to the high fuel flow rate. Comparing Figs. 4 and 5 reveals that fuel-lean combustion is more effective in improving OWMT, whereas fuel-rich combustion is beneficial to control the NO emission.

In ammonia combustion the mechanism of Fenimore NO is considered to be unimportant, due to the absence of radical CH responsible

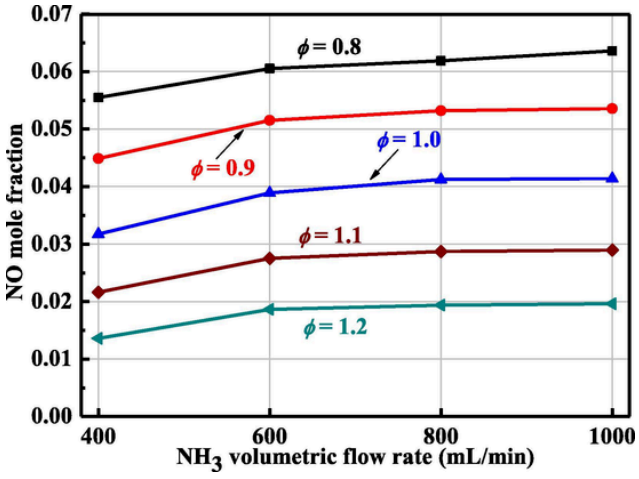

Fig. 5. The dependence of mole fraction of NO on the fuel flow rate for different ϕ.

for prompt NO [50]. Meanwhile, there is assumed to be no fuel-bound N in the present work, as the conversion of fuel-nitrogen, also called fuel-bound nitrogen (FBN), into NO is mainly observed in coal combustion. On the contrary, the Zeldovich NO (thermal NO) is believed to play a major role in the NO formation. The NO generation rate can be calculated by:

$$\frac{d[\mathrm{NO}]}{dt} = 2k_1\,[O]\,[N_2] \tag{7}$$

where $k_1$is the rate of reaction $N_2 + O = NO + N$ with a value of $1.8\times10^{14}\exp(-318kJ\bullet mol^{-1}/(RT))cm^3/(mol\bullet s)$; [NO], $[O]$ and $[N_2]$ are the molar concentrations.

As indicated in Eq. (7), NO can be minimized by decreasing $[O]$, $[N_2]$, or k_1(i.e., by decreasing the temperature). Therefore, it is of great importance to investigate the temperature distribution. Fig. 6 presents the temperature fields on the cross section as a function of ϕ, as the NH_3 volumetric flow rate is 600 mL/min. It can be seen that in ammonia-rich flames, the region with a high temperature near the outlet is much smaller compared to that of under fuel-lean conditions, mainly due to the incomplete combustion resulting from the deficiency in the oxidizer. These are qualitatively in accordance with the data shown in Fig. 4. Meanwhile, the decreased flame temperature is effective in reducing the NO generation rate, as NO formation is highly temperature sensitive. This explains why the NO production rate tends to decrease with increasing ϕ, as shown in Fig. 5. Furthermore, it is worth highlighting that although the flame temperature at $\phi = 0.9$ is higher than that of $\phi = 0.8$ at fuel-lean conditions, the NO emission is higher at $\phi = 0.8$, primarily because of the high O atom concentrations. These results suggest that the combined effects result in the significant decrease in the NO mole fraction with increasing the equivalence ratio. This is consistent with the findings discovered by Li et al. [51], They confirmed that a high fuel/oxidizer equivalence ratio was associated with a low NO formation rate.

3.2. Effect of the inlet temperature T_{in}

The thermodynamic properties such as the inlet temperature T_{in} and pressure P_{in} may affect the ammonia combustion, and thus thermal as well as emission performance. Let us first consider the effect of T_{in}. Fig. 7 shows the variation of OWMT varied with NH_3 volumetric flow rate, as T_{in} is set to 5 different values and $\phi = 1.0$. It can be seen that for a given value of T_{in}, OWMT is found to increase, as the NH_3 volumetric flow rate is increased. This is due to the large heat release rate resulting from the increased chemical energy input. Meanwhile, another unique feature illustrated in Fig. 7 is that OWMT changes remarkably with T_{in}. Increasing T_{in} is shown to be associated with a drop in the OWMT, suggesting that the OWMT is highly dependent on T_{in}.

To shed light on how the inlet temperature affects the thermal performance of such micro-combustor, the temperature contours on the cross-section as a function of T_{in} are illustrated in Fig. 8, when the NH_3 volumetric flow rate is 600 mL/min. It can be seen from the figure that the flame is almost similar in shape, i.e., the region of a high temperature occurs near the combustor inlet and a low temperature near the outlet. Nevertheless, it should be noted that the region of a high flame temperature varies in size and it shrinks with increasing T_{in}. Furthermore, a high T_{in} is found to be involved with a low temperature at the outlet. The decreased flame temperature is not favorable for transferring heat from the combustion products to the inner walls, thus leading to the low OWMT. These results are consistent with the data shown in Fig. 7, and indicates that the OWMT is a linear function of T_{in}.

Apart from OWMT, the NO mole fraction at the combustor outlet is also examined as a function of NH_3 volumetric flow rates at various T_{in} when $\phi = 1.0$. This is shown in Fig. 9. It can be seen from the figure that the NO concentrations vary considerably with T_{in}. That is, increasing T_{in} results in the NO production rate being decreased, which is similar to the variation of OWMT. The maximum decrease in the NO production rate can be up to 9.5%, as T_{in} is varied from 300 to 500 K. This is due to the fact that increasing the stream inlet temperature enable the flame velocity being increased, so that the flame is more likely to be located near the combustor inlet, as shown in Fig. 8. However, the region where the flame is anchored in is not beneficial on transferring the heat from the gas to the inner combustor walls, thus resulting in the low outer wall mean temperature. Meanwhile, the region with a high temperature is becoming narrower, which is advantageous for reducing the NO generation rate. Similar finding was reported by Sorrentino et al. [52]. They identified that preheating the inlet air flow allowed to reach a low NO_x emissions for stoichiometric mixtures. Furthermore, it is interesting to note that at a relatively low inlet temperature ($T_{\mathrm{in}} \le 350$ K) the NO concentrations vary non-monotonically as a function of the fuel flow rate. An increase in the NO generation rate can be observed when increasing the fuel flow rate from 400 mL/min to 800 mL/min. However, a further increase in the flow rate leads to a decrease in NO formation. This reveals that decreasing T_{in} can contribute to a lower NO production, especially at low NH_3 volumetric flow rates.

To gain a better understanding of how the T_{in} affects the NO_x emissions, we further explore the NO and OH contours. Comparison of NO and OH distributions as a function of T_{in} on the cross-section are shown in Fig. 10. It can be seen from Fig. 10 (a) that the distribution of NO profiles are the same in the shape, i.e., the region with a high NO concentration is located near the combustor inlet and the NO concentration is gradually decreased along the streamwise direction. This is quite reasonable, since the NO formation is closely associated with the flame temperature which tends to peak near the inlet as the chemical reaction occurs (shown in Fig. 8). It is, however, worth noting that there are

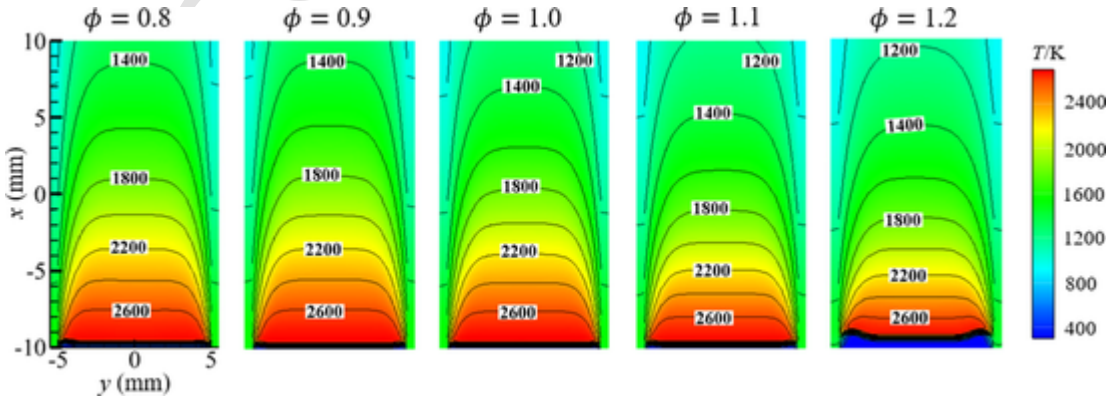

Fig. 6. Temperature field contours on cross-section at different ϕ, with the fuel flow rate being set to 600 mL/min.

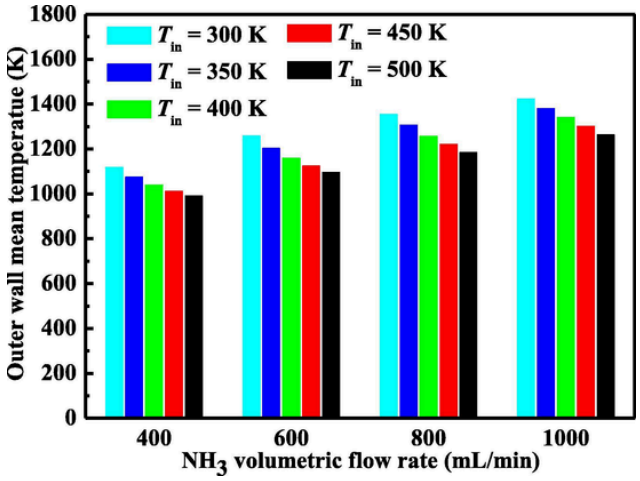

Fig. 7. Comparison of OWMT with varied NH_3 volumetric flow rate, as T_{in} is set to 5 different values.

considerable differences in the NO concentrations downstream of the micro-channel. Increasing the T_{in} is found to result in the region with a low NO concentration being enlarged. This is consistent with the results, as illustrated in Fig. 9. Since the NO formation is dependent on OH concentrations [27], it is of interest to investigate the OH distribution, as shown in Fig. 10 (b). It is clear that with increasing T_{in}, both the peak value of the OH concentration and its region are found to be smaller, which is beneficial for a low NO generation rate. Comparing Figs. 8 and 10 reveals that the small region of a high temperature and the low OH concentrations are responsible for the low NO_x emission at a high T_{in}.

3.3. Effect of the inlet pressure P_{in}

Now let us consider the effect of the inlet pressure P_{in} on determining the chemical reaction process and affecting micro-combustion phenomena. Fig. 11 illustrates the variations in the OWMT with various the fuel flow rates, as P_{in} is set to five different values ranging from 1.0 to 2.0 atm. As expected, at a given value of P_{in}, OWMT is shown to be higher with increasing the NH_3 flow rate, mainly because of the larger chemical energy input. This finding is similar to our previous results when discussing the effects of the equivalence ratio ϕ and the inlet temperature P_{in}. Furthermore, it is worth noting that OWMT is greatly affected by P_{in}. Increasing P_{in} is found to increase the OWMT significantly, irrespective of the NH_3 volumetric flow rate. Up to 224 K in the OWMT can be achieved, as P_{in} is varied from 1.0 to 2.0 atm. Therefore, it could be concluded that the inlet pressure plays a critical role in determining the outer wall temperature of such combustor.

To provide greater insight into the mechanism underlying the variation in the OWMT with varying the inlet pressure P_{in}, the temperature distributions on the cross-section of the combustor are explored, as shown in Fig. 12. It can be observed that the flame temperatures are similar in the shape with a high temperature upstream of the combustor and a low temperature downstream. Nevertheless, it is worth pointing out that the region of a high flame temperature varies significantly at different P_{in}. The region with a high flame temperature is found to become larger with increased P_{in}, indicating that a large P_{in} is able to promote the mixing and push the flame downstream. The enlarged region with a high flame temperature contributes to enhance the heat transfer between the mixed gases and the combustor inner walls, thereby leading to a high OWMT.

Given the variations in the combustor outer-wall temperature as P_{in} is varied, it is necessary to evaluate the effect of P_{in} on the NO emissions. Fig. 13 illustrates the NO concentrations on the combustor outlet as a function of the fuel flow rate with varied P_{in}. It is clear that in general, the NO concentrations tend to increase with increased the fuel flow rate, whatever the P_{in} is set to. This difference can be attributed to the increased flame temperature as a consequence of the high heat release rate. A closer observation on Fig. 13 shows that with the elevated P_{in}, the NO concentrations are significantly reduced. Up to 26.5% decrease in the NO mole fraction can be achieved with varying the P_{in}. This suggests that the NO generation rate is highly sensitive to the inlet pressure.

Consider the large variations in NO concentrations among different P_{in} on the combustor outlet, it is of great interest to investigate the NO and velocity distributions. Fig. 14 shows the contour distributions of (a) NO and (b) velocity field on the cross-section of the combustor under various P_{in}. From Fig. 14 (a), it can be seen that there is a region with a high NO concentration occurring near the combustor inlet, irrespective of the inlet pressure. These regions, however, are much smaller with increasing P_{in}, implying that a less NO is produced during the combustion. This is consistent with the finding illustrated in Fig. 13. Despite the presence of the high flame temperature at a large P_{in}, the residence time of combustion products with a high temperature inside the channel is relatively short as a results of the high flame velocity, as shown in Fig. 14 (b), which is responsible for the lower NO formation. Comparing Figs. 12 and 14 indicates that the NO formation is not only affected by the flame temperature but also the residence time.

To further illuminate how P_{in} affects the NO formation, the OH radical profile is studied, on which the NO production is strongly dependent on [27]. Fig. 15 illustrates the centerline OH mole fractions on the cross-section in the streamwise direction, as the NH_3 volumetric flow rate is set as 600 mL/min. It can be seen that the shape of the centerline OH profiles are almost the same in the five flames as P_{in} is varied, i.e., the mole fraction of OH is sharply increased first and then de-

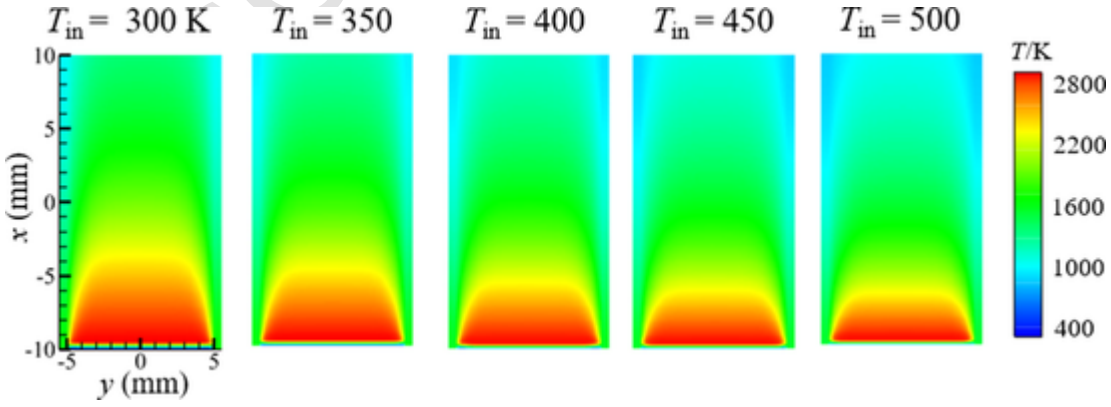

Fig. 8. Temperature field contours on the cross-section at various T_{in} with the fuel flow rate being set to 600 mL/min.

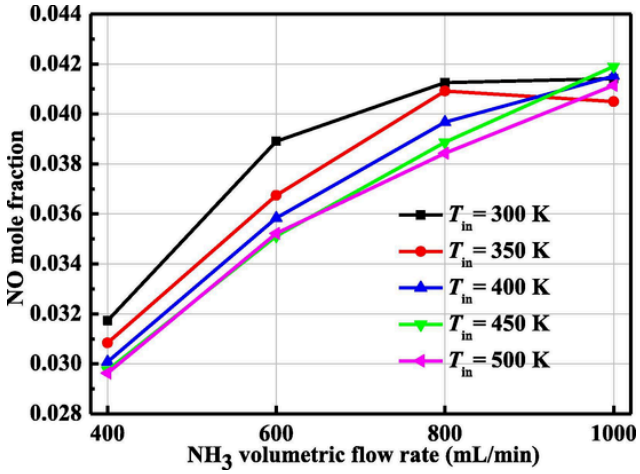

Fig. 9. The dependence of NO mole fraction on the fuel flow rate, as T_{in} is set to 5 different values.

cayed, as the chemical reaction takes place. However, there are significant differences regarding the amount of the OH concentrations for different P_{in}. Specifically, the higher the inlet pressure, the less the OH fraction, thus leading to the NO production being decreased. Therefore, it could be concluded that a higher inlet pressure plays a positive effect in enhancing chemical reaction, and thus the higher OWMT, and in reducing the NO generation due to the shortened residence time.

4. Conclusions

In the present work, thermal performances and NO emission characteristics of premixed ammonia/oxygen combustion in a micro-planar combustor are numerically studied. For this, a 3D computational model with detailed chemical kinetic mechanisms is developed and used to study the effects of 1) the equivalence ratio ϕ, 2) the combustor inlet temperatures T_{in} as well as 3) the inlet pressures P_{in}. The key findings are summarized as follows:

(1) The outer wall mean temperature (OWMT) varies non-monotonically, as the mixture varies from fuel-lean (ϕ<1.0) to fuel-rich (ϕ>1.0) conditions. It peaks at ϕ = 0.9, mainly due to the optimal heat transfer performance between the gases and the combustor walls.

(2) The NO production is highly dependent on ϕ. Decreasing ϕ is found to be associated with a high NO emission, with most effects being attributed to the increased flame temperature as well as the O atom. Up to 24.5% decrease in the NO concentrations can be achieved, as ϕ is optimized.

(3) The inlet temperature T_{in} plays a critical role in affecting the OWMT as well as NO production. Increasing T_{in} could lead to a decrease not only in the OWMT but also the NO concentration.

(4) A noticeable increase in the OWMT is observed, as the inlet pressure P_{in} is elevated. This is mostly because of the enhanced heat transfer caused by the intensified mixing process. Furthermore, due to the reduced residence time of the high temperature in the combustion passage, a high P_{in} is shown to be associated with a low NO emission.

The present work confirms that varying the combustor inlet thermodynamic properties is a feasible way to enhance thermal performances and reduce NO emissions from the perspectives of power output and environment issue.

Declaration of Competing Interest

The authors declare that they have no known competing financial interests or personal relationships that could have appeared to influence the work reported in this paper.

Acknowledgements

We gratefully acknowledge the financial support provided by the University of Canterbury, New Zealand (grant no. 452STUPDZ) and

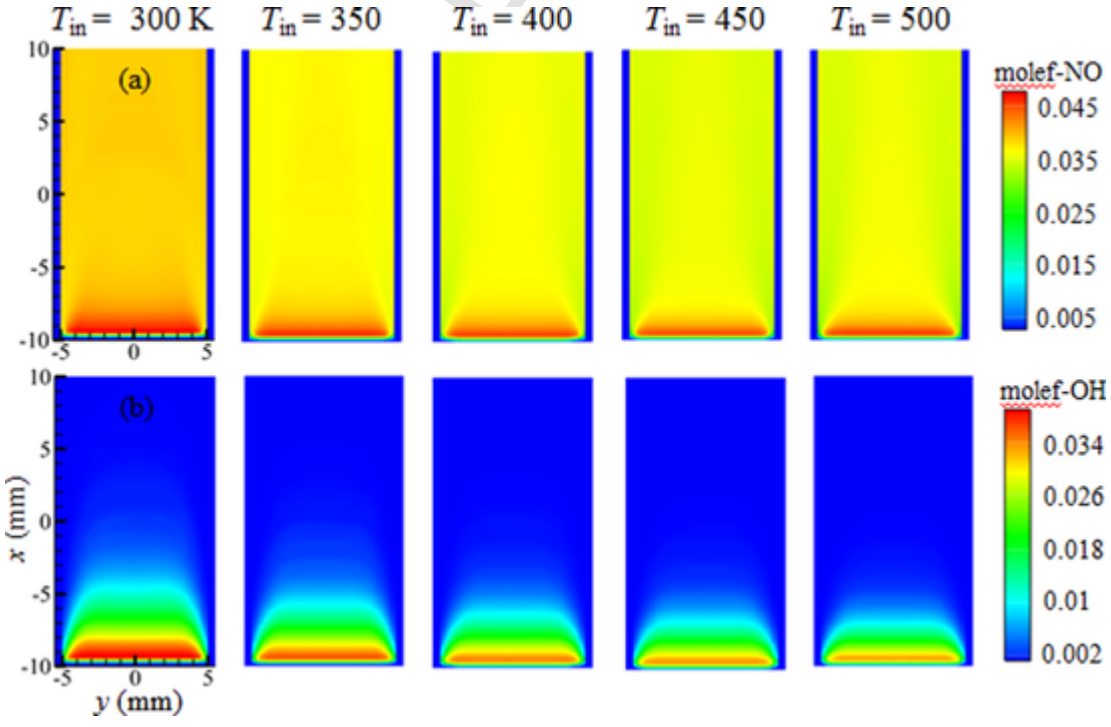

Fig. 10. Variation of distributions of (a) NO and (b) OH on the cross-section of the combustor at various T_{in}.

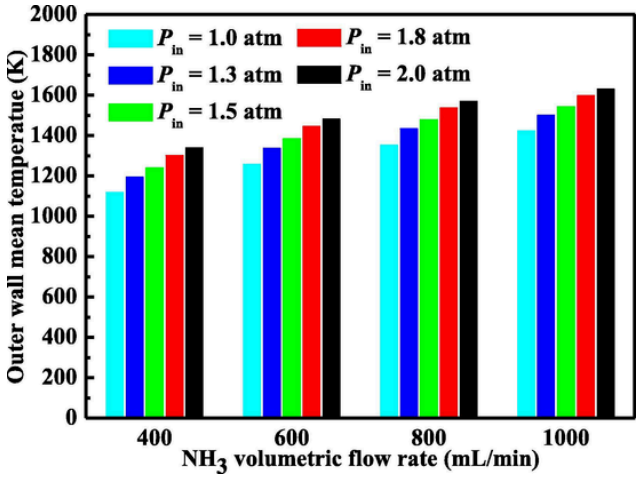

Fig. 11. Comparison of OWMT with varied fuel flow rates, as P_{in} is set to 5 different values.

Singapore National Research Foundation (grant no. NRF2016 NRF-NSFC001-102). Tao Cai would like to thank to College of Engineering, University of Canterbury for providing his PhD studentship.

Appendix A. Supplementary data

Supplementary data to this article can be found online at https://doi.org/10.1016/j.fuel.2020.118554.

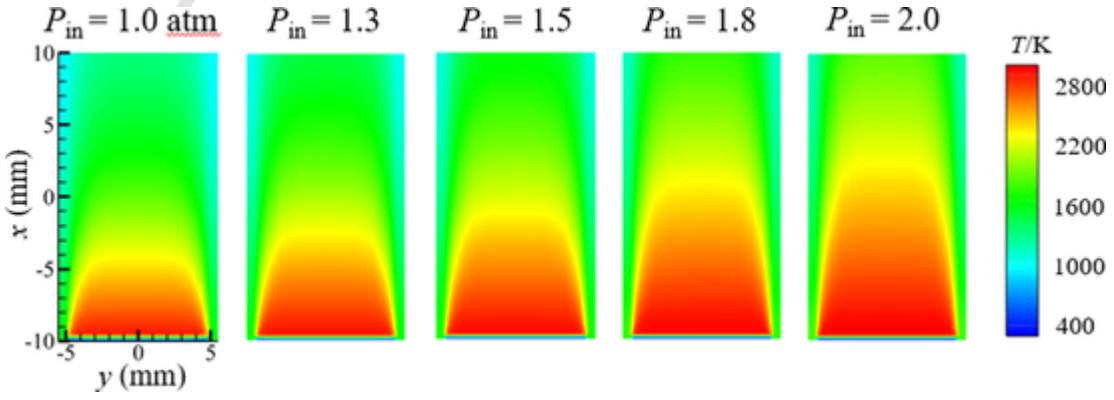

Fig. 12. Temperature field contours as a function of P_{in} with the fuel flow rate being set to 600 mL/min.

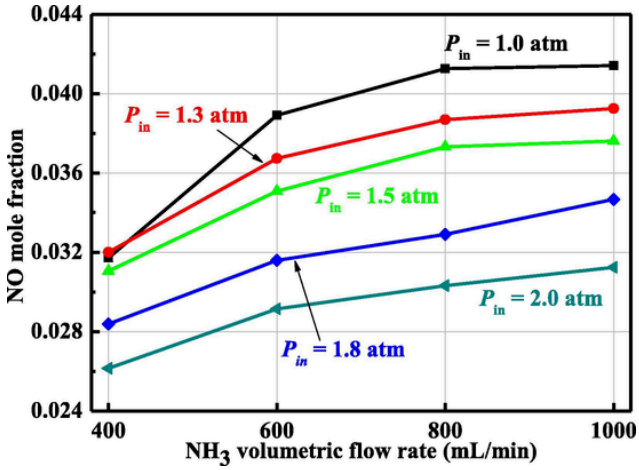

Fig. 13. The dependence of the NO mole fraction on the fuel flow rate, as P_{in} is set to 5 different values.

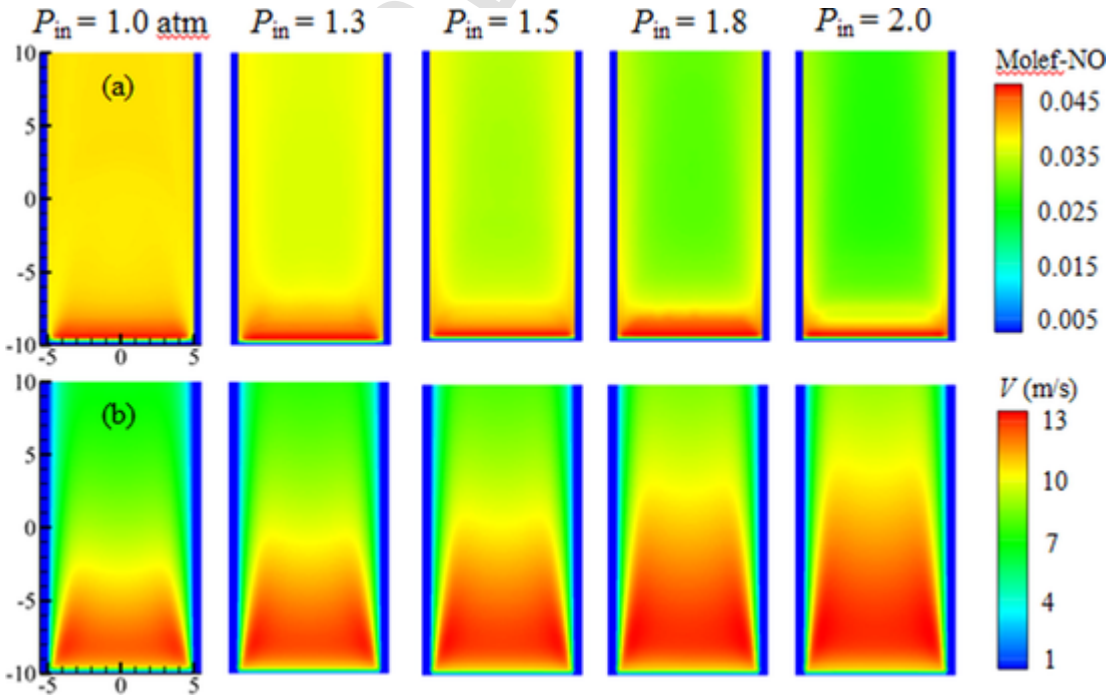

Fig. 14. Distributions of (a) NO and (b) velocity field on the cross-section of the combustor at various P_{in}.

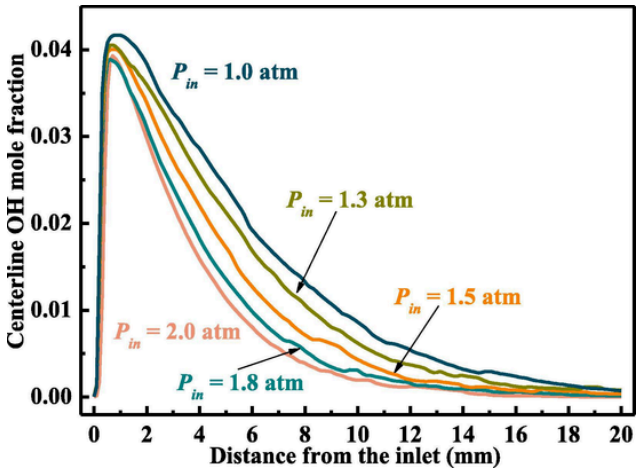

Fig. 15. Profiles of the centerline OH mole fractions on the cross-section along with the axial distance from the combustor inlet, as P_{in} is set to 5 different values.

References

[1] G R Astbury A review of the properties and hazards of some alternative fuels. Process Saf Environ Protect 2008;86(6):397–414.
[2] R F Service Ammonia-a renewable fuel made from sun, air, and water-could power the globe without carbon. Science 2018. doi:10.1126/science.aau7489.
[3] A Valera-Medina, H Xiao, M Owen-Jones, W I F David, P J Bowen Ammonia for power. Prog Energy Combust Sci 2018;69:63–102.
[4] J Li, H Y Huang, N Kobayashi, Z H He, Y Nagai Study on using hydrogen and ammonia as fuels: Combustion characteristics and NOx formation. Int J Energy Res 2014;38(9):1214–1223.
[5] C Zamfirescu, I Dincer Ammonia as a green fuel and hydrogen source for vehicular applications. Fuel Process Technol 2009;90(5):729–737.
[6] T Hejze, J O Besenhard, K Kordesch, M Cifrain, R R Aronsson Current status of combined systems using alkaline fuel cells and ammonia as a hydrogen carrier. J Power Sources 2008;176(2):490–493.
[7] W H Avery A role for ammonia in the hydrogen economy. Int J Hydrogen Energy 1988;13:761–773.
[8] Y Bicer, I Dincer, C Zamfirescu, G Vezina, F Raso Comparative life cycle assessment of various ammonia production methods. J Cleaner Prod 2016;135:1379–1395.
[9] H Ishaq, I Dincer Analysis and optimization for energy, cost and carbon emission of a solar driven steam-autothermal hybrid methane reforming for hydrogen, ammonia and power production. J Cleaner Prod 2019;234:242–257.
[10] E Kroch Ammonia-a fuel for motor buses. J Ins Pet 1945;31:213–223.
[11] E S Starkman, H K Newhall, R Sutton, T Maguire, L Farbar Ammonia as a spark ignition engine fuel: theory and application. SAE Technical Paper 1966;660155.
[12] Liu R, Ting D S-K, Checkel MD Ammonia as a fuel for SI engine. SAE Technical Paper 2003-1-3095; 2003.
[13] Duynslaegher C, Jeanmart H, Vandooren J. Use of ammonia as a fuel for SI engine. Proc European Combust Meeting; 2009.
[14] C Duynslaegher, H Jeanmart, J Vandooren Ammonia combustion at elevated pressure and temperature conditions. Fuel 2010;89(11):3540–3545.
[15] C Duynslaegher, F Contino, J Vandooren, H Jeanmart Modeling of ammonia combustion at low pressure. Combust Flame 2012;159(9):2799–2805.
[16] F R Westlye, A Ivarsson, J Schramm Experimental investigation of nitrogen based emissions from an ammonia fueled SI-engine. Fuel 2013;111:239–247.
[17] A A Boretti Novel heavy duty engine concept for operation dual fuel H_2-NH_3. Int J Hydrogen Energy 2012;37(9):7869–7876.
[18] A A Boretti Novel dual fuel diesel-ammonia combustion system in advanced TDI engines. Int J Hydrogen Energy 2017;42(10):7071–7076.
[19] C S Mørch, A Bjerre, M P Gøttrup, S C Sorenson, J Schramm Ammonia/hydrogen mixtures in an SI-engine: Engine performance and analysis of a proposed fuel system. Fuel 2011;90(2):854–864.
[20] K Ryu, G E Zacharakis-Jutz, S-C Kong Performance characteristics of compression-ignition engine using high concentration of ammonia mixed with dimethyl ether. Appl Energy 2014;113:488–499.
[21] K Ryu, G E Zacharakis-Jutz, S-C Kong Effects of gaseous ammonia direct injection on performance characteristics of a spark-ignition engine. Appl Energy 2014;116:206–215.
[22] A J Reiter, S-C Kong Demonstration of compression-ignition engine combustion using ammonia in reducing greenhouse gas emissions. Energy Fuels 2008;22:2963–2971.
[23] K D K A Somarathne, S Hatakeyama, A Hayakawa, H Kobayashi Numerical study of a low emission gas turbine like combustor for turbulent ammonia/air premixed swirl flames with a secondary air injection at high pressure. Int J Hydrogen Energy 2017;42(44):27388–27399.
[24] O Kurata, N Iki, T Matsunuma, T Inoue, T Tsujimura, H Furutani, et al. Performances and emission characteristics of NH_3-air and NH_3-CH_4-air combustion gas-turbine power generations. Proc Combust Inst 2017;36(3):3351–3359.
[25] K D K A Somarathne, S Colson, A Hayakawa, H Kobayashi Modelling of ammonia/air non-premixed turbulent swirling flames in a gas turbine-like combustor at various pressures. Combust Theory Modell 2018;22(5):973–997.
[26] A Hayakawa, Y Arakawa, R Mimoto, K D Kunkuma, A Somarathne, T Kudo, et al. Experimental investigation of stabilization and emission characteristics of ammonia/air premixed flames in a swirl combustor. Int J Hydrogen Energy 2017;42(19):14010–14018.
[27] K D K A Somarathne, E C Okafor, A Hayakawa, T Kudo, O Kurata, N Iki, et al. Emission characteristics of turbulent non-premixed ammonia/air and methane/air swirl flames through a rich-lean combustor under various wall thermal boundary conditions at high pressure. Combust Flame 2019;210:247–261.
[28] H Xiao, A Valera-Medina, P J Bowen, S Dooley 3D simulation of ammonia combustion in a lean premixed swirl burner. Energy Procedia 2017;142:1294–1299.
[29] O Kurata, N Iki, T Inoue, T Matsunuma, T Tsujimura, H Furutani, et al. Development of a wide range-operable, rich-lean low-NOx combustor for NH_3 fuel gas-turbine power generation. Proc Combust Inst 2019;37(4):4587–4595.
[30] H Xiao, A Valera-Medina, P J Bowen Modeling combustion of ammonia/hydrogen fuel blends under gas turbine conditions. Energy Fuels 2017;31(8):8631–8642.
[31] H Xiao, M Howard, A Valera-Medina, S Dooley, P J Bowen Study on reduced chemical mechanisms of ammonia/methane combustion under gas turbine conditions. Energy Fuels 2016;30(10):8701–8710.
[32] A Valera-Medina, D G Pugh, P Marsh, G Bulat, P Bowen Preliminary study on lean premixed combustion of ammonia-hydrogen for swirling gas turbine combustors. Int J Hydrogen Energy 2017;42(38):24495–24503.
[33] H Xiao, M S Howard, A Valera-Medina, S Dooley, P J Bowen Reduced chemical mechanisms for ammonia/methane co-firing for gas turbine applications. Energy Procedia 2017;105:1483–1488.
[34] N A Hussein, A Valera-Medina, A S Alsaegh Ammonia-hydrogen combustion in a swirl burner with reduction of NOx emissions. Energy Procedia 2019;158:2305–2310.
[35] Iki N, Kurata O, Matsunuma T, Inoue T, Suzuki M, Tsujimura T, Furutani H. Micro gas turbine firing kerosene and ammonia ASME Paper GT2015-43689; 2015.
[36] E C Okafor, K D K A Somarathne, R Ratthanan, A Hayakawa, T Kudo, O Kurata, et al. Control of NOx and other emissions in micro gas turbine combustors fuelled with mixtures of methane and ammonia. Combust Flame 2020;211:406–416.
[37] H Nakamura, S Hasegawa, T Tezuka Kinetic modeling of ammonia/air weak flames in a micro flow reactor with a controlled temperature profile. Combust Flame 2017;185:16–27.
[38] H Nakamura, S Hasegawa Combustion and ignition characteristics of ammonia/air mixtures in a micro flow reactor with a controlled temperature profile. Proc Combust Inst 2017;36(3):4217–4226.
[39] E C Okafor, K D K A Somarathne, A Kunkuma, A Hayakawa, T Kudo, O Kurata, et al. Towards the development of an efficient low-NOx ammonia combustor for a micro gas turbine. Proc Combust Inst 2019;37(4):4597–4606.
[40] Y G Ju, K Maruta Microscale combustion: Technology development and fundamental research. Prog Energy Combust Sci 2011;37(6):669–715.
[41] M C Drake, R J Blint Thermal NOx in stretched laminar opposed-flow diffusion flames with $CO/H_2/N_2$ fuel. Combust Flame 1989;76:151–167.
[42] ANSYS Fluent User's Guide, Release 18.1, ANSYS, Inc., April 2017.
[43] H Bongers, L P H De Goey The effect of simplified transport modeling on the burning velocity of laminar premixed flames. Combust Sci Technol 2003;175(10):1915–1928.
[44] L H Li, S X Wang, L Zhao, A Fan A numerical investigation on non-premixed catalytic combustion of $CH_4/(O_2+N_2)$ in a planar micro-combustor. Fuel 2019;255. doi:10.1016/j.fuel.2019.115823.
[45] Q G Peng, W M Yang, E Jiaqiang, H P Xu, Z W Li, K L Tay, et al. Investigation on premixed H_2/C_3H_8/air combustion in porous medium combustor for the micro thermophotovoltaic application. Appl Energy 2020;260. doi:10.1016/j.apenergy.2019.114352.
[46] J Li, S K Chou, Z W Li, W M Yang Characterization of wall temperature and radiation power through cylindrical dump micro-combustors. Combust Flame 2009;156(8):1587–1593.
[47] Q G Peng, E Jiaqiang, J W Chen, W Zuo, X H Zhao, Z Q Zhang Investigation on the effects of wall thickness and porous media on the thermal performance of a non-premixed hydrogen fueled cylindrical micro combustor. Energy Convers Manage 2018;155:276–286.
[48] P Glarborg, J A Miller, B Ruscic, S J Klippenstein Modeling nitrogen chemistry in combustion. Prog Energy Combust Sci 2018;67:31–68.
[49] G J Rortveit, J E Hustad, S C Li, F A Williams Effects of diluents on NO_x formation in hydrogen counter-flow flames. Combust Flame 2002;130:48–61.
[50] Warnatz J, Mass U, Dibble RW Combustion, Springer-Verlag, Berlin, 2006, 4th.
[51] J Li, H Y Huang, N Kobayashi, Z H He, Y Osaka, T Zeng Research on combustion and emission characteristics of ammonia under preheating conditions. J Chem Eng Japan 2016;49(7):641–648.
[52] G Sorrentino, P Sabia, P Bozza, R Ragucci, M Joannon Low-NOx conversion of pure ammonia in a cyclonic burner under locally diluted and preheated conditions. Appl Energy 2019;254. doi:10.1016/j.apenergy.2019.113676.